Motional Ground State Cooling Outside the Lamb-Dicke Regime

Y. Yu,[*] N. R. Hutzler,[†] J. T. Zhang, L. R. Liu, T. Rosenband, and K.-K. Ni[‡]

Department of Chemistry and Chemical Biology,
Harvard University, Cambridge, Massachusetts, 02138, USA
Department of Physics, Harvard University, Cambridge, Massachusetts, 02138, USA and
Harvard-MIT Center for Ultracold Atoms, Cambridge, Massachusetts, 02138, USA
(Dated: January 28, 2018)

We report Raman sideband cooling of a single sodium atom to its three-dimensional motional ground state in an optical tweezer. Despite a large Lamb-Dicke parameter, high initial temperature, and large differential light shifts between the excited state and the ground state, we achieve a ground state population of 93.5(7)% after 53 ms of cooling, for the 96% of atoms that survive re-imaging. Our technique includes addressing high-order sidebands, where several motional quanta are removed by a single laser pulse, and fast modulation of the optical tweezer intensity. We demonstrate that Raman sideband cooling to the 3D motional ground state is possible, even without tight confinement and low initial temperature.

Trapped neutral atoms, assembled in an array of optical tweezers, are a promising platform to study quantum information and quantum simulations [1–7]. The inherent single-particle detection and control, combined with tunable interactions, allow implementations of neutral-atom-based quantum logic gates [3, 4], novel quantum phases [6], and single-photon switches [8, 9]. Advances in real-time re-arrangement of optical tweezers enable rapid preparation of atoms in large and complex geometries [10, 11]. Quantum motional control of individual atoms [12–16] enable studies of the atomic Hong-Ou-Mandel effect [17], high-fidelity single qubit gates [18], and efficient coupling of single atoms to photonic crystal cavities [19].

Extending optical tweezer arrays to include polar molecules will open a range of new applications that exploit long-lived molecular internal states and tunable long range interactions [20–22]. Molecules could be assembled from atom pairs in optical tweezers [15], or directly loaded from magneto-optical traps (MOTs) [23–25]. For either approach, preparing the constituent atoms or molecules in the lowest motional quantum state is important to realize long coherence times in quantum applications.

Preparation of single atoms in the motional ground state has been achieved in optical tweezers [13–16] using Raman sideband cooling (RSC) [26–28]. However, RSC in these systems takes place in the Lamb-Dicke (LD) regime, where the spread of the initial wavefunctions is smaller than the reduced wavelength of light (λ) used to address them. Systems with a large position spread (z_{rms}), either due to small mass or high initial temperature, fall outside of the LD regime and undergo strong recoil heating during RSC. In this letter we demonstrate cooling of single sodium atoms in optical tweezers, initially outside the LD regime ($z_{\mathrm{rms}}/\lambda = 4.0$), to the motional ground state. We achieve a 3D ground state population of $P_0 = 93.5(7)\%$ by cooling via high-order sidebands in a carefully optimized cooling sequence. Our

approach is general and applicable to other systems. Extending RSC beyond the LD regime opens the possibility for ground state cooling of systems such as light atoms and molecules that can be laser-cooled.

Our experiment has an overall repetition rate of 2.5 Hz and begins by loading a single sodium atom into an optical tweezer from a MOT [29]. The tweezer is created by focussing a 700 nm wavelength laser beam through an NA=0.55 objective to an elliptical waist with radii $\{w_{0,x}, w_{0,y}\} \approx \{0.70, 0.69\}\,\mu$m. For 45 mW of optical power, the trapping frequencies along the three axes are $\{\omega_x, \omega_y, \omega_z\}/2\pi = \{479(4), 492(5), 86(1)\}$ kHz, where z is the weakly confined axial direction, and x and y are the tightly confined radial directions. After each single atom loading attempt, a first image is taken with a 1.5 ms exposure time to determine success, which occurs about 50% of the time due to the loading mechanism [1]. During imaging, the atom is cooled via polarization gradient cooling (PGC), which reduces the temperature of the single atom to 80 μK, corresponding to mean motional states along the three trap axes of $\{\bar{n}_x, \bar{n}_y, \bar{n}_z\} = \{3.5(3), 3.2(3), 20(4)\}$, and therefore initial 3D ground state probability of $P_0 = 0.4\%$. The atom is then initialized into the $|F = 2, m_F = 2\rangle$ stretched state via optical pumping (OP). Each experimental cycle ends with a second imaging sequence that measures the hyperfine state of the atom as $|F = 2\rangle$ or $|F = 1\rangle$ [30]. The data analysis includes only those experiments where the first image reveals successful atom loading.

To reduce the temperature of the single atom and achieve high ground state population, we apply Raman sideband cooling [13, 26]. The energy levels, cooling sequence, and Raman beam geometries are shown in Fig. 1. RSC consists of two steps: driving a coherent Raman transition to remove motional quanta, followed by resetting the atom's internal state via OP. These steps are repeated, until the motional ground state is populated with high probability.

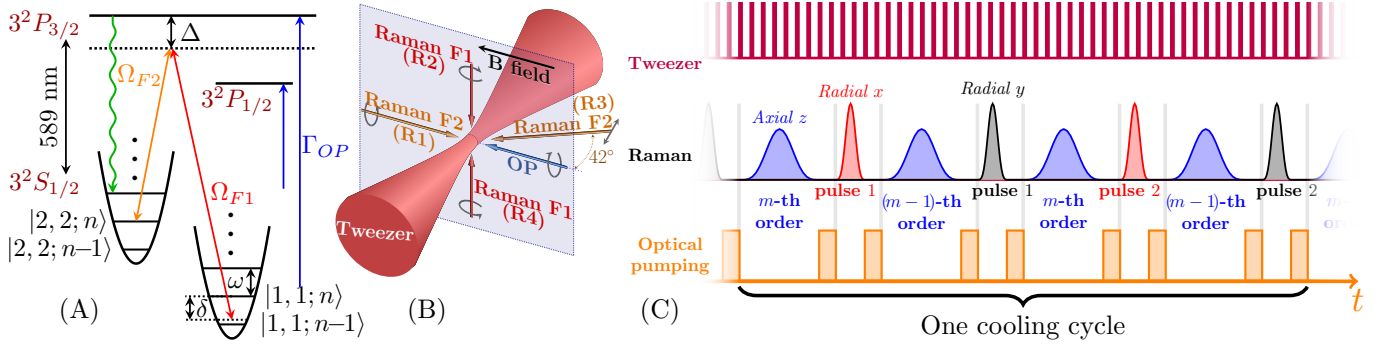Specifically, Raman transitions are driven in ^{23}Na be-

FIG. 1. Single Na atom Raman sideband cooling scheme and sequence. (A) The Raman transitions between $|2,2;n\rangle$ and $|1,1;n+\Delta n\rangle$ have a one-photon detuning $\Delta = 75$ GHz below the $3^2S_{1/2}$ to $3^2P_{3/2}$ transition. Two-photon detuning, δ, is defined relative to the $\Delta n = 0$ carrier transition. For optical pumping, we use two σ^+ polarized transitions, one to pump the atom state out of $|1,1\rangle$ via $3^2P_{3/2}$ and one to pump atoms out of $|2,1\rangle$ via $3^2P_{1/2}$ to minimize heating of the $|2,2\rangle$ state. (B) Geometry and polarizations of the Raman and optical pumping beams relative to the optical tweezer and bias magnetic field. Raman beams R1 and R4 address the radial x-mode. R1 and R2 address the radial y-mode. R3 and R4 address the axial z-mode, where the beams also couple to radial motion, but this coupling can be neglected when the atoms is cooled to the ground state of motion. (C) Schematic of the cooling pulse sequence. The tweezer is strobed at 3 MHz to reduce light shifts during optical pumping [29]. Each cooling cycle consists of 8 sideband pulses. The four axial pulses address two sideband orders. The two pulses in each radial direction either address $\Delta n = -2$ and $\Delta n = -1$ or have different durations to drive $\Delta n = -1$, at the end of the cooling sequence when most of the population is below $n = 3$. The Raman cooling and spectroscopy pulses have Blackman envelopes [31] to reduce off-resonant coupling, while the measurement Rabi pulses in Fig. 3(B,C) and 4(B,C) have square envelopes to simplify analysis.

tween the hyperfine states $|2,2\rangle$ and $|1,1\rangle$ in the presence of an 8.8 G magnetic field. The external field is orthogonal to the effective magnetic field of the tweezer, to reduce vector light shifts [13, 14]. Subsequently, an OP pulse, which consists of two frequencies both with σ^+-polarization, is applied to bring the atom out of the $F = 1$ manifold and back to $|2,2\rangle$ via spontaneous emission (Fig. 1A). It is important that the optical pumping step scatter as few photons as possible to minimize recoil heating. Therefore, to optically pump atoms from $|2,1\rangle$ into $|2,2\rangle$ while keeping the target state dark, we apply light resonant with $3^2P_{1/2}$ [26, 32] [33].

During optical pumping, photon recoil can lead to significant heating, especially along the weakly-confined axial direction (z). For an atom starting in an axial motional level n_{init}, the probability to end in another axial state n after absorbing and re-emitting one photon is approximated by an angular integral of the squared matrix element $|\langle n_{\text{init}}|e^{i\Delta k_{\text{OP}}z}|n\rangle|^2$ [34]. Here Δk_{OP} is the wave vector difference between absorbed and emitted photons, projected onto the z-axis. As shown in Fig. 2A, the probability of gaining motional energy during OP grows with n_{init}, and is an important effect for sideband-cooling outside the Lamb-Dicke regime.

Fortunately, the large LD parameters in our system also provide opportunities to overcome OP heating. The LD parameter for Raman transitions is defined as $\eta^{\text{R}} \equiv \Delta k z_0$, where Δk is the wave vector difference between the two beams that drive the Raman transition. Here $z_0 = \sqrt{\hbar/(2m\omega)}$ is the ground state wavefunction spread (m is the atomic mass). The Ra-

man transitions in our configuration have LD parameters of $\{\eta_x^{\text{R}}, \eta_y^{\text{R}}, \eta_z^{\text{R}}\} = \{0.323(2), 0.319(1), 0.36(1)\}$. To offset heating from OP initially when n is large, higher-order Raman sidebands ($|\Delta n| > 1$) remove several motional
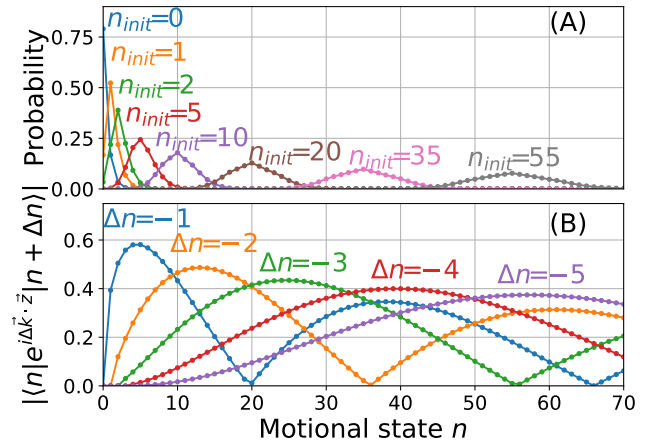

FIG. 2. Optical pumping motional-state redistribution and Raman coupling for large LD parameters for the axial direction (z). The range plotted covers 95% of the initial thermal distribution. (A) Motional state distribution after one OP cycle for different initial states motion, n_{init}. Due to photon-recoil and the large LD parameter, $\eta_z^{\text{OP}} = 0.55$, there is a high probability of n changing. (B) Matrix elements for Raman transition deviate from $\sqrt{n}$ scaling with multiple minima. During cooling, we utilize the fact that high motional states couple most effectively to sidebands with large $|\Delta n|$.

quanta in a single cooling pulse (see Fig. 2B). Because the coupling strengths of different orders do not reach minima for the same state of motion n, using multiple orders of sidebands avoids accumulations of population near the coupling minima.

Taking the large motional-state changing heating and cooling sources into account, it is not immediately clear that ground-state cooling can be achieved. We therefore use a Monte-Carlo simulation to guide our search [35]. In particular, we find that alternating the cooling pulses (Fig. 1C) between two neighboring orders for the axial direction and $\Delta n = -2$ and $\Delta n = -1$ for the radial directions eliminates the accumulation of population in motional states that have zero Raman coupling, which would halt the cooling process. The simulation also indicates that setting the coupling strength of each sideband to drive a Rabi π-pulse corresponding to the maximum matrix element motional state (i.e. the maxima in Fig. 2B) yields efficient cooling, initially. The efficiency of cooling on higher-order sidebands diminishes as the atom approaches the ground state, so the final cycles utilize only the $\Delta n = -1$ sideband while alternating between the three axes.

Guided by the simulation results, we construct our axial cooling sequence by starting at the two highest observed sideband orders ($\Delta n = -5$ and $\Delta n = -4$) and decreasing the orders to the next pair after every 6 to 15 cycles. This process is repeated until $\Delta n = -1$, and most of the population is in the first few excited states. We then switch to cooling only on $\Delta n = -1$ with two different pulse lengths in order to efficiently cool atoms in the few remaining motional states. Radial cooling is performed similarly to axial cooling with the initial cooling of $\Delta n = -2$ and $\Delta n = -1$ and switching to $\Delta n = -1$ only after 20 to 30 pulses. This sequence gives good initial cooling performance, which is then used to calibrate experimental parameters, including the Rabi rates of the Raman beams and optical pumping rates.

There are two additional important challenges in cooling single sodium atoms. First, the initial temperature populates high motional states, causing the atoms to sample the anharmonicity of the trap away from the center. Anharmonicity may be defined as $A_{i,n} = (E_{i,n+1} - E_{i,n})/h - \omega_i/(2\pi)$ for each trap axis i, and calculated from the quartic term of the optical tweezers via perturbation theory. In the paraxial approximation, we find $A_{i,n} = \frac{-3n\hbar}{4\pi m d_i^2}$, where d_i equals the beam radius for the radial directions and $d_z \approx \pi w_{0,x} w_{0,y}/\lambda_{\mathrm{trap}}$. Numerically, $\{A_{x,n}, A_{y,n}, A_{z,n}\} = \{-1.4, -1.4, -0.16\}n$ kHz. For mixed states, this broadens high-order sidebands due to the n-dependence of the transitions. In order to mitigate this, we drive the sidebands with a large Rabi frequency and short pulses to Fourier broaden the spectrum. However, anharmonicity may still shift high-n states out of resonance and prevent effective cooling.

Second, the tweezers cause a large light shift (as large as 300 MHz) in the excited state. We address this by strobing the trapping light at a rate of 3 MHz during the whole cooling sequence, similar to our loading and imaging process [29], while leaving OP on with constant intensity. Due to the large light shift, the OP is effectively off whenever the trap light is on. Since the atom is still addressed by optical pumping light when the trap light is off, OP remains effective.

Our final cooling results are shown in Fig. 3 and 4. In total, 540 cooling pulses (total duration 53 ms) are applied along three axes with cooling beginning on the radial second order and axial eighth order. The full RSC pulse sequence is given in [37]. To characterize the single atom thermal state before and after cooling, we perform Raman sideband thermometry [26, 36]. For the more tightly confined (non-degenerate) radial directions, we observe clear $\Delta n = 1$, $\Delta n = -1$, and $\Delta n = -2$ sidebands before RSC, as is shown in Fig. 3A. After RSC, the $\Delta n = -1$ and $\Delta n = -2$ sidebands on both radial axes are strongly reduced. The formula that equates the ratio of $\Delta n = -1$ and $\Delta n = 1$ sideband heights to $\bar{n}/(\bar{n}+1)$ ($\bar{n}$ is the mean motional quantum number of the assumed thermal state) was derived in the LD regime [26]. However, it is also valid outside the LD regime. The resulting $\bar{n}_x = 0.019(4)$ and $\bar{n}_y = 0.024(3)$ correspond to ground-state fractions of 98.1(5)% and 97.6(3)%, in agreement with fitted values of 98(1)% and 95(3)% from the Rabi flopping curves [36] in Fig. 3B and 3C. The initial temperature of $80 \, \mu$K before RSC is obtained from similar fits.

For the weak axial direction, cooling is challenging because the atom starts outside the LD regime. We observe up to 5th-order Raman cooling sidebands initially, which indicates population in highly-excited motional states. Nevertheless, our cooling sequence works efficiently as all the $\Delta n < 0$ sidebands are reduced after RSC (Fig. 4A). Using the ratio of first-order sideband heights, we obtain $\bar{n}_z = 0.024(5)$, which corresponds to a ground state population of 97.6(5)%, in agreement with a ground state population of 95(4)% extracted from Rabi flopping when $\Delta n = 0$ (Fig. 4B). For the $\Delta n = 1$ sideband (Fig. 4C), we observe additional decoherence that is more pronounced due to the slower Rabi frequency. The decoherence rate is consistent with magnetic field fluctuations of 1.5 mG measured independently in the lab, which would produce a Zeeman shift of ~ 3 kHz.

Combining the axial and radial cooling results, a single Na atom is in the 3D ground state with a probability of 93.5(7)% after RSC. We note that there is an additional 4% population loss from imaging. The cooling efficiency is limited by spontaneous scattering rate (0.1-0.2 kHz) from the Raman beams, as well as spectral broadening from magnetic field fluctuations and trap anharmonicity.

We measure a heating rate that corresponds to decreasing 3D ground state population at a rate of $\sim 0.9\%$/ms.
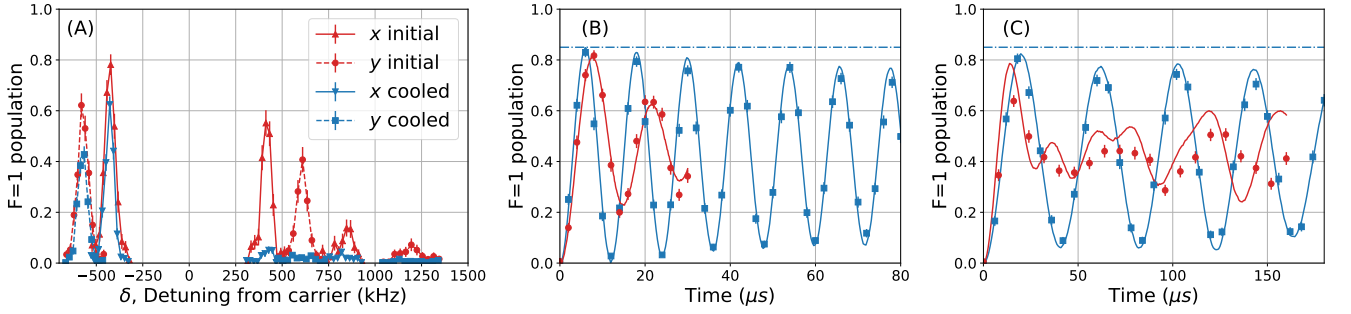
FIG. 3. (A) Left to right: Radial Raman sideband spectrum of $\Delta n_y = 1$, $\Delta n_x = 1$, $\Delta n_x = -1$, $\Delta n_y = -1$, $\Delta n_x = -2$, $\Delta n_y = -2$ before and after Raman sideband cooling. (B,C) Rabi flopping on axis y (B) carrier and (C) $\Delta n_y = 1$ sideband before (red circle) and after (blue square) RSC. Solid lines in (B) and (C) are fits to a Rabi-flopping that includes a thermal distribution of motional states [36] as well as off-resonant scattering from the Raman beams. The blue lines correspond to a 1D ground state probability of 98.1% after cooling and the red lines correspond to a thermal distribution of 80 μK before RSC.
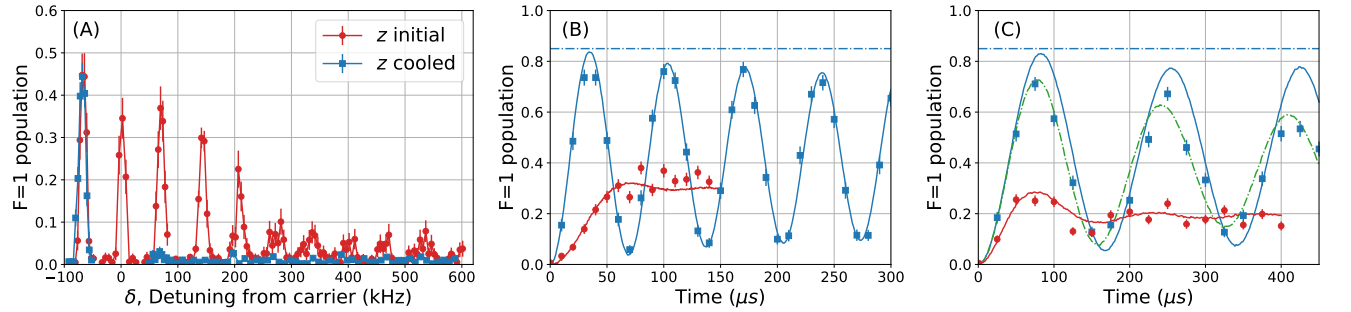

FIG. 4. (A) Left to right: Axial Raman sideband spectrum from $\Delta n_z = 1, 0, -1, \ldots, -5$ before and after Raman sideband cooling. (B,C) Rabi flopping on axial (B) carrier $\Delta n_z = 0$ and (C) $\Delta n_z = 1$ sideband before (red circle) and after (blue square) RSC. Solid blue lines in (B) and (C), similar to Fig. 3B and C, are fits to the Rabi flopping and yield a ground state probability of 95% after cooling and the red lines correspond to a thermal distribution of 80 μK before RSC. The green line in (C), includes the additional decoherence due to a fluctuation of the hyperfine splitting of magnitude 3 kHz. We see that the decoherence effect is strongest for the post-cooling data on the $\Delta n_z = 1$ sideband where the Rabi frequency is the lowest.

The rate is consistent with off-resonant scattering of the trapping light [38], and is predominantly in the axial direction where the trapping beam propagates.

We expect to enhance the ground state probability after RSC by increasing the detuning of the Raman beams, addressing a wider range of axial trap anharmonicity, implementing better control of the magnetic field, and optimizing imaging. Another improvement could be to implement grey molasses cooling to achieve a lower starting temperature before RSC [39].

We have shown that despite the difficulty in achieving a low optical cooling temperature of low mass sodium atoms, three dimensional cooling with significant ground state population can be achieved by using high-order Raman sidebands in an optimized cooling sequence. These techniques are well-suited for a large variety of systems and open up a route to ground state cooling for other species, including molecules and exotic atoms.

We thank J. D. Hood for discussions. This work is supported by the Arnold and Mabel Beckman Foundation, the AFOSR Young Investigator Program, the NSF

through the CUA, and the Alfred P. Sloan Foundation.

* yichaoyu@g.harvard.edu
† Present address: California Institute of Technology, Division of Physics, Mathematics, and Astronomy. Pasadena, CA, 91125
‡ ni@chemistry.harvard.edu

[1] N. Schlosser, G. Reymond, I. Protsenko, and P. Grangier, Nature **411**, 1024 (2001).
[2] D. S. Weiss, J. Vala, A. V. Thapliyal, S. Myrgren, U. Vazirani, and K. B. Whaley, Phys. Rev. A **70**, 040302 (2004).
[3] L. Isenhower, E. Urban, X. L. Zhang, A. T. Gill, T. Henage, T. A. Johnson, T. G. Walker, and M. Saffman, Phys. Rev. Lett. **104**, 010503 (2010).
[4] T. Wilk, A. Gaëtan, C. Evellin, J. Wolters, Y. Miroshnychenko, P. Grangier, and A. Browaeys, Phys. Rev. Lett. **104**, 010502 (2010).
[5] A. M. Kaufman, B. J. Lester, M. Foss-Feig, M. L. Wall, A. M. Rey, and C. A. Regal, Nature **527**, 208 (2015).
[6] H. Labuhn, D. Barredo, S. Ravets, S. de Léséleuc,

T. Macrì, T. Lahaye, and A. Browaeys, Nature **534**, 667 (2015).

[7] S. Murmann, A. Bergschneider, V. M. Klinkhamer, G. Zürn, T. Lompe, and S. Jochim, Phys. Rev. Lett. **114**, 080402 (2015).

[8] B. Dayan, A. S. Parkins, T. Aoki, E. P. Ostby, K. J. Vahala, and H. J. Kimble, Science **319**, 1062 (2008).

[9] T. G. Tiecke, J. D. Thompson, N. P. de Leon, L. R. Liu, V. Vuletić, and M. D. Lukin, Nature **508**, 241 (2014).

[10] D. Barredo, S. de Léséleuc, V. Lienhard, T. Lahaye, and A. Browaeys, Science **354**, 1021 (2016).

[11] M. Endres, H. Bernien, A. Keesling, H. Levine, E. R. Anschuetz, A. Krajenbrink, C. Senko, V. Vuletic, M. Greiner, and M. D. Lukin, Science **354**, 1024 (2016).

[12] X. Li, T. A. Corcovilos, Y. Wang, and D. S. Weiss, Phys. Rev. Lett. **108**, 103001 (2012).

[13] A. M. Kaufman, B. J. Lester, and C. A. Regal, Phys. Rev. X **2**, 041014 (2012).

[14] J. D. Thompson, T. G. Tiecke, A. S. Zibrov, V. Vuletić, and M. D. Lukin, Phys. Rev. Lett. **110**, 133001 (2013).

[15] L. R. Liu, J. T. Zhang, Y. Y. Yu, N. R. Hutzler, Y. Liu, T. Rosenband, and K.-K. Ni, arXiv 1701.03121 (2017).

[16] C. Robens, J. Zopes, W. Alt, S. Brakhane, D. Meschede, and A. Alberti, Phys. Rev. Lett. **118**, 065302 (2017).

[17] A. M. Kaufman, B. J. Lester, C. M. Reynolds, M. L. Wall, M. Foss-Feig, K. R. A. Hazzard, A. M. Rey, and C. A. Regal, Science **345**, 306 (2014).

[18] Y. Wang, A. Kumar, T.-Y. Wu, and D. S. Weiss, Science **352**, 1562 (2016).

[19] J. D. Thompson, T. G. Tiecke, N. P. de Leon, J. Feist, A. V. Akimov, M. Gullans, A. S. Zibrov, V. Vuletic, and M. D. Lukin, Science **340**, 1202 (2013).

[20] D. DeMille, Phys. Rev. Lett. **88**, 067901 (2002).

[21] A. V. Gorshkov, S. R. Manmana, G. Chen, E. Demler, M. D. Lukin, and A. M. Rey, Phys. Rev. A **84**, 033619 (2011).

[22] B. Yan, S. A. Moses, B. Gadway, J. P. Covey, K. R. A. Hazzard, A. M. Rey, D. S. Jin, and J. Ye, Nature **501**, 521 (2013).

[23] J. F. Barry, D. J. McCarron, E. B. Norrgard, M. H. Stei-necker, and D. DeMille, Nature **512**, 286 (2014).

[24] S. Truppe, H. J. Williams, M. Hambach, L. Caldwell, N. J. Fitch, E. A. Hinds, B. E. Sauer, and M. R. Tarbutt, (2017), arXiv:1703.00580.

[25] L. Anderegg, B. Augenbraun, E. Chae, B. Hemmerling, N. R. Hutzler, A. Ravi, A. Collopy, J. Ye, W. Ketterle, and J. Doyle, (2017), arXiv:1705.10288.

[26] C. Monroe, D. M. Meekhof, B. E. King, S. R. Jefferts, W. M. Itano, D. J. Wineland, and P. Gould, Phys. Rev. Lett. **75**, 4011 (1995).

[27] A. J. Kerman, V. Vuletić, C. Chin, and S. Chu, Phys. Rev. Lett. **84**, 439 (2000).

[28] D.-J. Han, S. Wolf, S. Oliver, C. McCormick, M. T. DePue, and D. S. Weiss, Phys. Rev. Lett. **85**, 724 (2000).

[29] N. R. Hutzler, L. R. Liu, Y. Yu, and K.-K. Ni, New J. Phys. **19**, 023007 (2017).

[30] The final hyperfine state sensitive detection employs a strong beam that is resonant with the $F = 2$ to $F' = 3$ cycling transition, to heat the $F = 2$ population out of the trap. Therefore, any atoms which survive this heat out procedure are interpreted as having been in the $F = 1$ state.

[31] M. Kasevich and S. Chu, Phys. Rev. Lett. **69**, 1741 (1992).

[32] M. Gröbner, P. Weinmann, E. Kirilov, and H.-C. Nägerl, Phys. Rev. A **95**, 033412 (2017).

[33] We find a reduction in the scattering rate by a factor of 130(20), as compared to using an OP resonant with $3^2 P_{3/2}$, from which the $|2, -2>$ state could always scatter a photon via the excited $|F' = 3, m_{F'} = -3>$ state.

[34] D. J. Wineland and W. M. Itano, Phys. Rev. A **20**, 1521 (1979).

[35] J. Dalibard, Y. Castin, and K. Mølmer, Phys. Rev. Lett. **68**, 580 (1992).

[36] D. M. Meekhof, C. Monroe, B. E. King, W. M. Itano, and D. J. Wineland, Phys. Rev. Lett. **76**, 1796 (1996).

[37] See supplemental material.

[38] R. Grimm, M. Weidemüller, and Y. B. Ovchinnikov, Adv. At. Mol. Opt. Phys. **42**, 95 (2000).

[39] G. Colzi, G. Durastante, E. Fava, S. Serafini, G. Lamporesi, and G. Ferrari, Phys. Rev. A **93**, 023421 (2016).